Electrical Power and Energy Systems 176 (2026) 111744

Contents lists available at ScienceDirect

International Journal of Electrical Power and Energy Systems

journal homepage: www.elsevier.com/locate/ijepes

Photovoltaic system reduces grid voltage waveform distortions in the frequency range from 700 Hz to 1250 Hz

Ellen Förstner *, Mohamad Dughmosh, Ralf Mikut, Karl-Heinz Haefele, Denis Jakel, Kaibin Bao, Heiko Maaß, Richard Jumar, Andreas Fotler, Uwe Kühnapfel, Veit Hagenmeyer

Karlsruhe Institute for Technology, Hermann-von-Helmholtz-Platz 1, Eggenstein-Leopoldshafen, 76344, Germany

ARTICLE INFO

Dataset link: https://doi.org/10.5281/zenodo.16306034

Keywords:
Photovoltaic
Voltage waveform distortions
Field measurement
Distortion reduction
High frequency resolution

ABSTRACT

Waveform distortions of voltages and currents are a recurring concern in the context of Photovoltaic (PV) systems. Reports exist where large PV systems shut down because of increasingly large grid voltage distortions. Due to the complexity of the system (PV installation and grid) it is difficult to discern whether the PV system generates or just amplifies a distortion. Frequencies observed in these events are various, come from both harmonic and interharmonic regimes, and call for a frequency-sensitive analysis. However, studies that investigate PV systems in the context of waveform distortions often focus on total distortion values. As a result, reports on the impact of PV installations on the Total Harmonic Voltage Distortion (THD_V) are inconsistent. Increasing, decreasing, and negligible effects on THD_V are observed.

We investigate the impact of a PV system in the field and keep a spectral perspective as opposed to aggregated values such as THD_V. Due to repeated shut-downs and power-ups of the system over the course of two days, we ensure to attribute observed effects to the system under investigation (and not other loads in the grid). We observe that voltage waveform distortions in the range from 700 Hz to 1250 Hz are reduced whenever the PV-system is connected to the grid, while distortions at other frequencies are increased or not affected. The impact of the PV system on voltage waveform distortions is frequency sensitive, and thus aggregated total distortion values are not a suitable measure in this context.

1. Introduction

Due to their inherent working principles, inverters can cause challenges such as the introduction or amplification of harmful distortions. Grid voltages and currents are superimposed with distortion frequencies. These include integer multiples of the fundamental frequency (50 Hz) called harmonics and non-integer multiples referred to as interharmonics.

Cases where inverters cause tremendous voltage distortions, triggering systems to shut down, have been reported [1–5]. These events raise concerns about the reliability of the future energy grid and highlight the system-level impact individual Photovoltaic (PV) systems can have on grid operation. In this context, it is important to investigate Photovoltaic (PV) installations and their impact on grid operation directly in-field, as opposed to detached laboratory or digital simulation conditions. The following literature review focuses on field measurements and excludes laboratory studies and simulations.

Overall, investigations on the impact of PV inverters on the grid voltage in-field are scarce. Acero et al. (2020) investigated a PV system in Peru and found that the Total Harmonic Voltage Distortion (THD_V) is smaller in the case of low power injection [6]. However, their analysis focuses mostly on current distortion and does not include individual harmonic voltages. Other authors report an increased Total Harmonic Voltage Distortion (THD_V) at low PV power output [7,8]. For example, a study by Al-Madjidi et al. (2021) in Great Britain compares data from a sunny and a cloudy day [7]. They find that THD_V is slightly larger on the cloudy day with less PV power injection. Both [7,8] calculate individual harmonic components, but their analysis focuses on the current distortions. Another field study by Adebiyi et al. (2023) found that THD_V is constant over the day and thus does not depend on PV power [9] and as such agrees with [10]. While all previous reports correlate voltage distortion with PV power, the effects cannot be attributed to the PV system directly. Other loads following similar temporal behavior might also affect THD_V. In contrast, Ahmed et al. (2017) investigated how power quality parameters changed before and after a PV system was installed at their institute in Egypt [11]. Their data shows, that THD_V decreased after the PV system was installed. Similar results, but comparing night and day data, can be found in [12,

* Corresponding author.
E-mail address: ellen.foerstner@kit.edu (E. Förstner).

https://doi.org/10.1016/j.ijepes.2026.111744
Received 14 August 2025; Received in revised form 30 January 2026; Accepted 27 February 2026
Available online 10 March 2026

13]. In these cases, the changes in distortions are more likely linked to the presence of the PV system. However, the studies still lack a broad spectral analysis. Individual harmonic voltages are calculated but not investigated towards their dependence on the presence of the PV system.

Overall, available field studies focus on the inverter current instead of grid voltage. They lack or do not fully exploit spectral depth but focus on total distortion values. Observed effects are not clearly attributed to the PV installation.

The present paper contributes to understanding the impact of PV installations on the public grid voltage distortions by adding spectral depth to the investigations. To this end, we perform measurements on our institute's PV installation under a dedicated test scenario that allows us to clearly attribute observed dependencies to the system under investigation. Section 2 describes the investigated PV system and measurement scenario, followed by the performed data analysis in Section 3. Section 4 presents the effect the PV system has on the voltage waveform distortion, and together with Section 5 interprets and discusses the observed frequency-dependency.

2. Investigated PV system and description of test scenario

We investigate the PV system on the roof of one of our institute buildings at the north campus of the Karlsruhe Institute of Technology (KIT) close to Karlsruhe, Germany. The system includes a total of 208 PV panels with a power output of 64.48 kW peak and feeds into the public grid via four inverters. The storage system installed next to the PV system is disconnected for the duration of the measurements in order to avoid interference with the measurement and will not be discussed further.

The main axis of the building is oriented roughly 15 degrees east with respect to the north-south axis. The arrangement of the PV panels on the flat roof is in line with the main axis of the building (azimuth angle = 15°) and is inclined (tilted) alternately to the east and west by a tilt angle of 10° to the horizontal.

The used PV panels model is IBC MonoSol 310 OS5, they possess a maximum power of 310 W under Standard Test Conditions (STC) and Normal Operating Cell Temperature (NOCT) with nominal voltage and current of 33 V and 9.4 A. The three-phase, transformer-less inverters are of type SMA STP 15000TL. Each inverter possesses a rated power of 15 kW and a maximum efficiency of 98.4 %.

The measurement process is designed to systematically assess the impact of the described PV system on voltage waveform distortions in the low-voltage grid. Other grid-connected consumers may also contribute to the overall voltage waveform, meaning that the PV system is not the sole factor influencing voltage distortions.

We measure three-phase AC voltages using the Electrical Data Recorder (EDR) [14,15]. The measurements are carried out between inverter 3 of the PV system and the busbar for the grid connection. Fig. 1 illustrates the measuring points between the inverters and the busbar. This placement ensures a direct observation of voltage waveforms at the grid coupling point while minimizing potential external interferences. Inverter 3 was selected solely based on the best connection options for measuring windings. The EDR continuously records the voltages at a sampling rate of 25 kHz. This high-frequency acquisition allows for a detailed spectral analysis, particularly in the frequency range relevant to harmonic and interharmonic distortion studies. Simultaneously with the EDR voltage measurements, the 15 s power reports as acquired within the inverters themselves are recorded.[1]

Our measurements last over two consecutive days, specifically a weekday (Friday, 20th of September, 2024) and a weekend day (Saturday, 21st of September, 2024). Both days are characterized by clear and stable weather conditions.

During the two measurement days, the PV system is repeatedly switched off for five minutes and subsequently switched on again for the next seven minutes, following a structured switching cycle from 9 am to 5 pm Central European Summer Time (CEST). These intervals ensure stable operating states are reached for *PV on* and *PV off*. In addition, we ensure to not synchronize our switching with the 15 min energy trading interval, thus reducing its possible influence on the observations. The state of the PV inverters is controlled via Modbus on the local network. Their communication interfaces implement the Sunspec specification, which was later standardized as IEEE 1547.[2] Specifically, we use holding register 40018 for fast shutdown. All Modbus interactions were scheduled using GNU's at daemon, and there was no need to use an SMA Grid Guard Code [18]. The Modbus commands were re-sent up to 3 times, as the communication was not always reliable.

3. Data analysis

Our analysis focuses, if not otherwise mentioned, on the voltage of phase A at inverter 3 during the period of switching operations on both measurement days (7 am to 3 pm Universal Time Coordinated (UTC), 9 am through 5 pm CEST, respectively). The analysis is performed in Matlab [19]. In short, we perform repeated Fourier analysis on 200 ms windows of data, average the spectra over each measurement interval (states *PV on* or *PV off*), and compare changes in the spectrum due to the disconnection of the PV system. In detail, the analysis consists of the following three steps:

1. Exact determination of switching times based on power data. The switching times are determined by applying a threshold of 100 W to the power data available for all four inverters individually. Fig. 2 exemplarily shows the power profiles on the second measurement day. The switching events are clearly visible as repeated power drops to zero for all four inverters. The overall reduced power output and later onset of power production in the early morning of inverters 3 and 4 is due to the positioning of the modules connected to these inverters. They are located on the north side and are more affected by shading.

The four different inverters do not always shut down at the same time. Start and end times of states are defined as the first time stamp at which all four inverters report power above/below the threshold. The orange (PV on) and purple (PV off) colors mark the analyzed time ranges for each state. For the exact start and end times of the measurement intervals in each state, the reader is referred to our published data repository [20].

2. Spectral analysis of voltage data. (a) Identification of the positive zero-crossings of the signal to identify full periods. (b) Segmentation of data into 200 ms windows while ensuring only full periods are included in an interval to reduce leakage. Usage of 200 ms Fourier windows is common practice as suggested in [21]. (c) Resampling of the data to 2^{11} samples for the benefit of Fast Fourier Transform (FFT) algorithm. (d) Multiplication of the data with the Hanning window function to further reduce leakage. (e) Transformation to the frequency domain using a FFT algorithm on each 200 ms interval. This results in a time series of spectral components $\mathcal{V}_f(t)$. Based on the Fourier interval of 200 ms, the frequency resolution is 5 Hz and five spectra per second are available. (f) Multiplication of the resulting spectrum with the Hanning window correction factor of two [22]. (g) Aggregation of spectral components up to 40th harmonic order (2 kHz) into harmonic $\mathcal{V}_{\mathrm{sg},h}(t)$ and interharmonic $\mathcal{V}_{\mathrm{isg},h}(t)$ subgroups according to IEC 61000-4-7 [21]. The order h corresponds to the frequency of the component (multiples of the fundamental frequency, 50 Hz). In case of interharmonics, order h refers to the components between the hth and $(h+1)$-th harmonic. Subgroups are a popular parameter [21,23] and make our work comparable to other investigations.

[1] The reports are transferred to a database via the Modbus protocol.

[2] Scripts are based on previous work by [16,17]

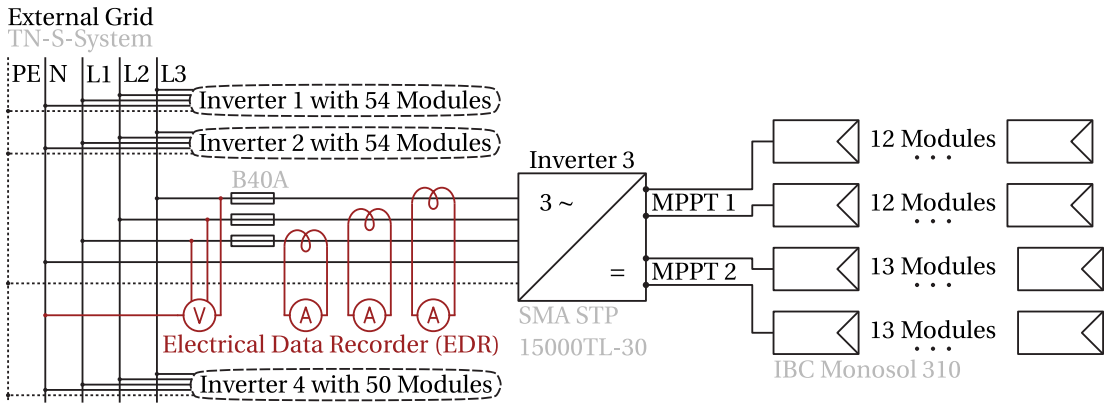

Fig. 1. Circuit Diagram of Investigated PV System. The measurements were taken at the connection point of inverter 3. Inverters 1, 2, and 4 are interconnected in the same way, and are here represented by the dashed ovals.

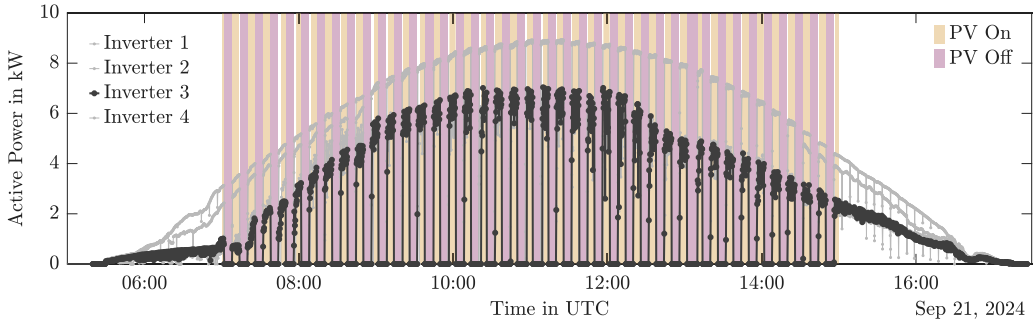

Fig. 2. PV Power shows the repeated shutdowns and power-ups performed during one of the two measurement days. The white regions of the data are excluded from analysis to ensure the system is fully powered up/down during the analyzed intervals.

3. Averaging of spectra over each measurement interval (states PV on and PV off separately). First, the spectra are assigned to the states *PV on* or *PV off*, based on the intervals identified in Fig. 2. Second, we average (mean) the spectra for each kth measurement interval of *PV on* and *PV off*. Small buffers of data are excluded at the start and end of the intervals (10 s around power up, 2 s around shut down. We end up with aggregated spectra $\overline{\mathcal{V}}^k_{Y,\,PV\,on/PV\,off}$. Y stands for individual spectral components, harmonic, or interharmonic subgroups.

4. Results

In addition to the spectral information, we also calculate the traditional aggregated measures for waveform distortions. These are the Total Harmonic Subgroup Distortion ($\mathrm{THDS_V}$) as defined in IEC 6100-4-7 [21] and the Total Interharmonic Subgroup Distortion ($\mathrm{TIHDS_V}$) as defined in in [23]. In the grid without the PV system, the voltage distortions on average are THDS = 3.30 %, and TIHDS = 0.16 %. Whenever the PV system is connected, the voltage distortions aggregate to THDS = 3.39 %, and TIHDS = 0.15 %. The changes in total distortion values are small, especially in case of interharmonics.

However, we do not want to exclude the possibility that the PV system significantly influences voltage waveform distortions. Thus, we expand our analysis to a full spectral perspective and look at how the disconnection of the PV system alters different frequency regions. For a look into the distribution of $\mathrm{THDS_V}$ and $\mathrm{TIHDS_V}$ the reader is referred to Figs. 4(a) and 4(b). Fig. 4 compares these two traditional distortion parameters with the new spectral evaluation presented in this paper.

The absolute spectra for each state *PV on* and *PV off* all look quite similar (compare additional figures in the data repository [20]). Among the overall diverse distortions present in the grid, the impact of the PV system is difficult to discern. To highlight the impact of the PV system we calculate the relative spectral differences for each shut-down event:

$$\Delta^k_{\mathrm{rel,Y}} = 2 \cdot \frac{\overline{\mathcal{V}}^k_{Y,\,PV\,on} - \overline{\mathcal{V}}^k_{Y,\,PV\,off}}{\overline{\mathcal{V}}^k_{Y,\,PV\,on} + \overline{\mathcal{V}}^k_{Y,\,PV\,off}} \tag{1}$$

There is a total of 80 shut-down events over the two measurement days.

4.1. Active PV system reduces distortions between 700 and 1250 Hz by more than 10%

We present the median differences over all shut-down events, including 5 % to 95 % percentiles in Fig. 3. The figure shows the differences $\Delta^k_{\mathrm{rel,f}}$ based on the individual spectral components (high spectral resolution) in Fig. 3(a). Fig. 3(b) shows the aggregation $\Delta^k_{\mathrm{rel,sg}}$ into subgroups. The underlying absolute amplitudes $\overline{\mathcal{V}}^k_f$ are shown in Fig. 3(c).

The upper plot shows positive and negative median differences between individual spectral components $\mathcal{V}_f(t)$. Most values are arranged in a band that follows a distinct frequency dependence, with only individual components (harmonics) outside of the band. The gray percentile range follows the course of the band but with greater dispersion at low and high frequencies. Based on the definition in Eq. (1), negative differences represent a reduction of distortions at respective frequencies due to the PV system being active, positive differences, instead, signify increased distortions at these frequencies when the PV system is active. The most prominent observation is the range of differences smaller than −10 % from 700 Hz to 1250 Hz with up to 40 % reduction at roughly 1000 Hz. The percentile range confirms this behavior, as the deviations mostly span closely around the median. At low frequencies between 0 Hz to 350 Hz, the median differences are consistently positive above 3 % but with broad uncertainty. This hints at a negative (increasing)

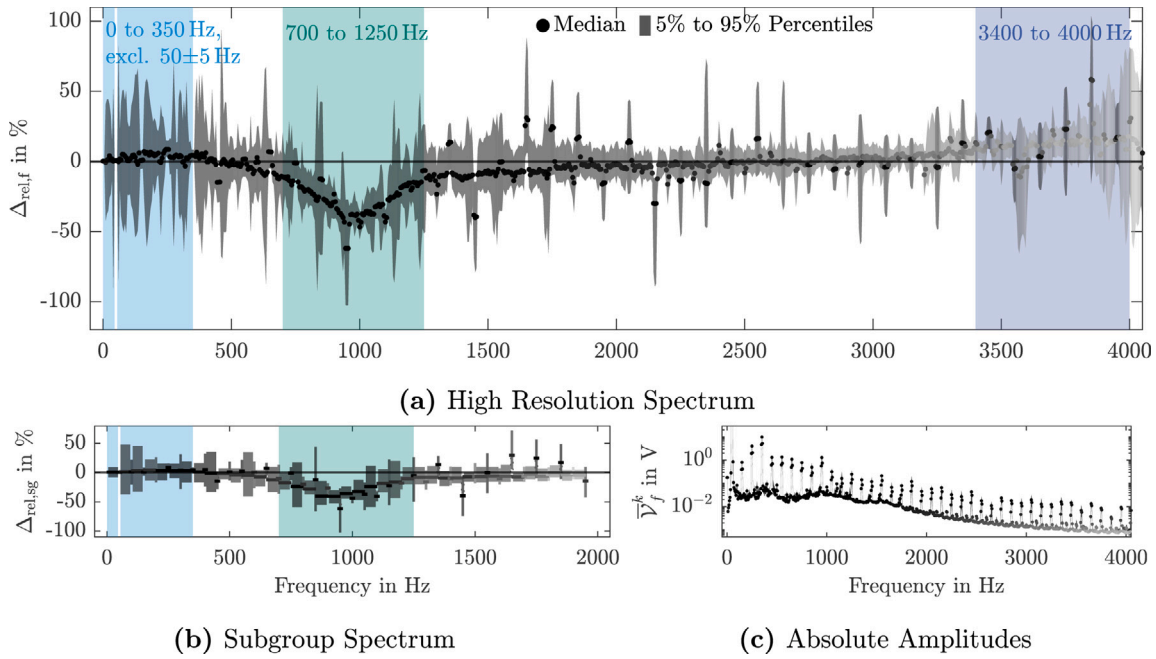

Fig. 3. Median relative difference of 80 shutdown events shows a clear tendency for frequencies from 700 Hz to 1250 Hz to be reduced due to the PV installation. The upper Fig. 3(a) shows the differences in high spectral resolution (5 Hz), Fig. 3(b) shows the data aggregated into harmonic and interharmonic subgroups up to 2000 Hz. For reference, the absolute amplitudes of the spectral components are visualized in Fig. 3(c). The amplitudes are also encoded in the brightness of the data in all three plots. Components with larger amplitudes are depicted in darker color as they contribute more to the overall distortion.

effect of an active PV system on the voltage waveform distortions in these frequencies. Similar observations hold for frequencies above 3.4 kHz. At other frequencies, the differences are close to zero, and the percentiles span both the positive and negative sides.

The significance of the relative difference values also depends on the underlying absolute amplitude of the component. These amplitudes are shown in the small axes on the right. They decrease with frequency, highlighting that frequencies up to 2 kHz contribute most to the voltage distortion. Harmonic distortions are higher compared to interharmonic frequencies. The amplitude is also highlighted in the brightness of all portrayed data. Frequencies with higher amplitude are more visible due to a darker color.

The differences for harmonic and interharmonic subgroups are calculated separately and are shown in the lower plot in Fig. 3. Each subgroup is displayed as a horizontal line in its respective frequency range. Interharmonics span over a larger frequency range and are thus represented by broader lines. They highlight that the components which diverge from the overall behavior are all from the harmonic regime.

In summary, the data shows a positive (reductive) influence of the active PV system on the grid voltage in the frequency range from 700 Hz to 1250 Hz on the voltage waveform distortions. All 80 shutdowns and both days agree on this behavior. Only the data of phase A is presented here. An identical analysis of the other two phases yields the same results.

4.2. Smaller impact at lower and higher frequencies

We further analyze the identified frequency ranges. For each spectrum individually, the components in three different frequency ranges are summed up (excluding fundamental frequency 50 ± 15 Hz from summation in the low-frequency range). As a result, we have the Partial Spectral Content (PSC):

$$\mathrm{PSC}_{0\,\mathrm{Hz}\ \text{to}\ 350\,\mathrm{Hz}}(t) = \sum_{f=0\,\mathrm{Hz}}^{350\,\mathrm{Hz}} \mathcal{V}_f(t) - \sum_{f=35\,\mathrm{Hz}}^{65\,\mathrm{Hz}} \mathcal{V}_f(t) \tag{2}$$

$$\mathrm{PSC}_{700\,\mathrm{Hz}\ \text{to}\ 1250\,\mathrm{Hz}}(t) = \sum_{f=700\,\mathrm{Hz}}^{1250\,\mathrm{Hz}} \mathcal{V}_f(t) \tag{3}$$

$$\mathrm{PSC}_{3.4\,\mathrm{kHz}\ \text{to}\ 4\,\mathrm{kHz}}(t) = \sum_{f=3.4\,\mathrm{kHz}}^{4\,\mathrm{kHz}} \mathcal{V}_f(t) \tag{4}$$

These time series of PSC are separated into the individual datasets for the two states *PV on* and *PV off*. No aggregation in time of the data (averaging) occurs; the full, high-resolution time-series is simply tagged with the different measurement states.

Fig. 4 shows the distributions of traditional total distortion parameters ($\mathrm{THDS_V}$ and $\mathrm{TIHDS_V}$) and the new PSC. The distributions for the two states *PV on* versus *PV off* are compared. None of the resulting datasets is normally distributed. Figs. 4(c) through 4(e) show the distribution of the PSC. In the low frequency range, the spectral content shows two very distinct peaks that do not overlap. The medium and high frequency ranges also show two peaks, but closer together and overlapping. In agreement with the average presented at the beginning of this section, the $\mathrm{THDS_V}$ distribution in Fig. 4(a) is shifted to higher values when the PV system is active. The $\mathrm{TIHDS_V}$ distribution in Fig. 4(b) shows lower values with PV system. In contrast, the shift in the PSC depends on the frequency range. The distributions in low and high frequencies are shifted to larger values when the PV system is active, while the shift in the medium frequency range is towards lower values. In addition, the distortions in the medium frequency range overlap much less. This highlights the significant impact the PV system has on distortions in the medium frequency range.

Wilcoxon rank sum tests on the PSC in the three different frequency ranges, each comparing data from the states *PV on* vs *PV off*, give the same result: The hypothesis that the two distributions (*PV on* and *PV off*) have the same median is rejected at the 5% significance level. The p-values are also the same $p = 0$ for each test. In other words, all three frequency ranges have deviating medians for the two different states *PV on* and *PV off*. For all frequency ranges, the difference between the states is significant, but the magnitude of the difference depends on frequency.

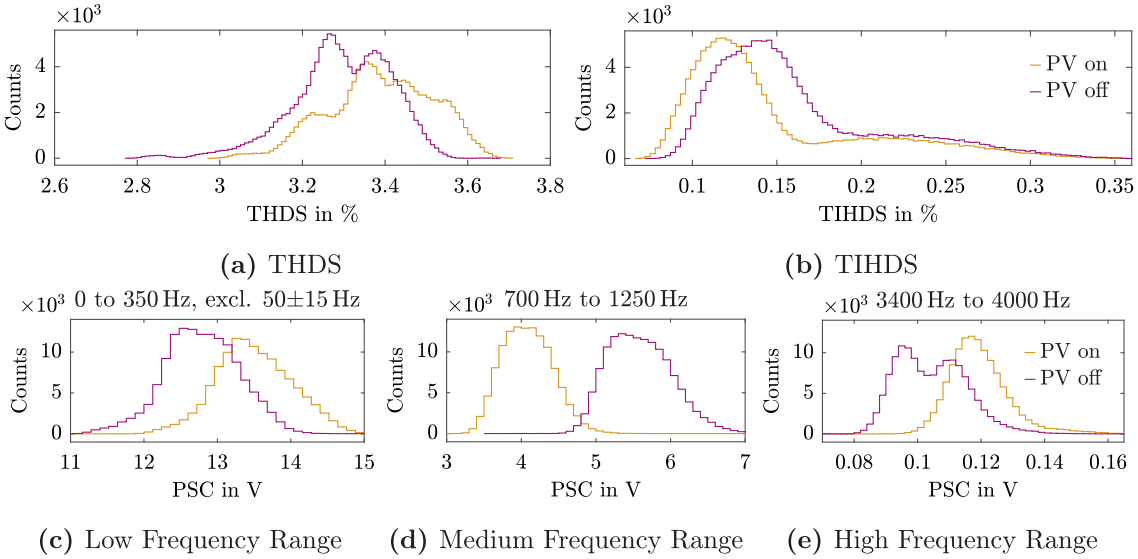

Fig. 4. Distributions of PSC shift in different directions depending on the frequency rang when the PV system is disconnected. The distribution of $THDS_V$ in Fig. 4(a) shifts to larger values when the PV system is connected, while the $TIHDS_V$ in Fig. 4(b) shifts to lower values. Figs. 4(c) through 4(e) show the distributions for the PSC in three different frequency ranges. The low and high frequency range shift to larger values when the PV system is connected. In contrast, the medium frequency range is reduced and the distributions show almost no overlap for the two states. This frequency-dependence is not captured in the shift of total distortion parameter distributions in the upper row.

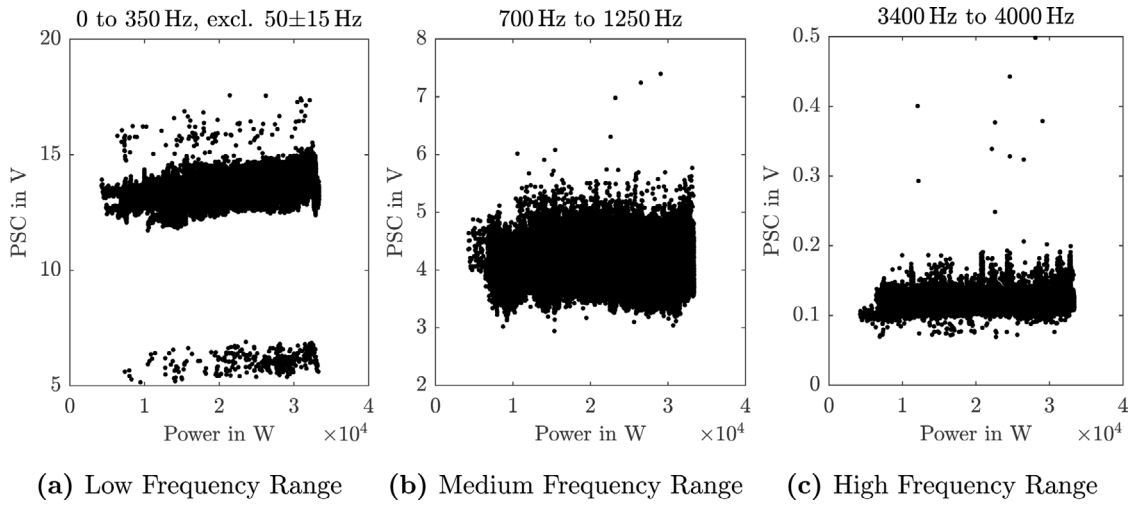

Fig. 5. PSC is independent from PV power. The scatter plots of the three frequency ranges as defined in Eqs. (2) through (4) show no dependence of power but broad distribution or different levels.

4.3. Partial spectral content is independent from PV power

The literature review in the Introduction shows, that contradicting impacts of the PV power on voltage waveform distortions are reported. We also investigate the impact of the power output of our PV system on the spectral content in the three different frequency ranges.

Fig. 5 shows the PSC over PV power. For the figure, only the data for the state *PV on* was used, as for *PV off*, naturally, the power is zero. The power value displayed on the x-axis is the sum of power input by all four inverters of the PV system. The PSC shows large dispersion, as can also be seen in the distributions in Figs. 4(c) through 4(e). In the low frequency range, the PSC also shows several values distinctively smaller than the rest of the times. These points amount to 0.3 % of the total data and represent individual spectra scattered over both measurement days with significantly reduced spectral content in the low frequency range. Especially due to the overall broad distributions, the power does not show any clear impact on the distortions. The PSC in the different frequency ranges appears independent of power. All changes observed between the distortions in the states *PV on* versus *PV off* can be attributed to the activity of the PV system (connected versus not connected), but not its power output.

5. Discussion

Previous investigations of waveform distortions in the context of PV installations often focus on current distortions. Any field-studies that do include voltage distortions either do not clearly attribute observed dependencies to the PV system or lack spectral depth and only focus on total distortion values or individual harmonics.

Our field-study focuses on voltage waveform distortions and maintains a spectral view, including various harmonic and interharmonic components. We can confirm that the analyzed PV system has both a

reductive and amplifying effect on voltage distortions simultaneously. A positive (reductive) impact is observed between 700 Hz to 1250 Hz, while increases in distortions occur at frequencies below 350 Hz and above 3.4 kHz. Overall, this leads to a slight increase in total harmonic content when the PV system is connected. However, the aggregated total distortion is incapable of displaying the underlying complex frequency-sensitive characteristic. The effect is independent of PV power output and depends solely on the presence (or absence) of the PV system.

Our observations are consistent over all 80 shutdown events at different times of day, power levels, and days. Our experimental setup, including the repeated deactivation of the PV system, allows us to compare two different system states (*PV on/PV off*) with a small intermediate time delay. We thus ensure that the observed effects are attributed to the PV system and not to other components in the system.

Possible root causes for observations include the passive filter components of the inverter, as well as active current injections due to control mechanisms. Presented observations are limited to a single PV installation within one specific network setting and thus cannot directly be applied to other systems. We assume the frequency-dependence to be different for other PV system and network characteristics. Especially, the frequency ranges chosen for deeper investigation in the PSC have to be chosen individually for each system under investigation.

Waveform distortions in power signals cause various problems, such as unwanted heating, disruption of measurements, and interference with communication. As a result, various mitigation strategies are investigated and many focus on PV installations [24]. The potential of PV system to not harm but, indeed, support sustainable and resilient grid operation has been recognized [25]. We observe a reductive impact of our PV system on voltage distortions around 1000 Hz. This offers the potential to extend grid supporting services of PV systems towards filtering waveform distortions.

In light of the identified frequency-dependent influence of PV systems on voltage waveform distortions and resulting unpredictable manifestation in less detailed parameters such as THD_V, future investigations should always include a detailed spectral view.

6. Conclusion

This paper applies an in-depth, frequency-sensitive investigation on a PV installation in-field. As such, it goes beyond available works that traditionally focus on inverter current instead of grid voltage, use aggregated total distortion values as opposed to a spectral view, and do not clearly attribute changes to the system under investigation by excluding other potential root causes. Our method shows that the investigated PV installation decreases voltage waveform distortions in the range of 700 Hz to 1250 Hz while introducing distortions at other frequencies. This proves that the effect of the PV system on the voltage of the grid is, in fact, frequency-sensitive.

The cause for the observed behavior is likely found either in the passive filter of the inverters or active current injections caused by the control scheme. These parameters and their impact depend very much on the individual system. So we predict different frequency ranges and magnitudes of the reductive and increasing influences on the distortion for different installations. Reductive and increasing effects at different frequencies, unique for each installation in its particular grid, could add up to either an overall positive or negative total distortion. As such, THD_V is an inadequate parameter to describe the impact of PV systems on grid voltage waveform distortions.

The frequency-sensitivity of the effect plays a decisive role in two aspects of larger grid studies: First, in interaction with other installations, the knowledge on the individual and joined characteristics of the systems allows more precise predictions on the occurrence of resonances and overall distortion levels. Second, the in-fact positive (reductive) impact of the PV system on voltage waveform distortions can be used specifically to control distortion levels in the grid by tuning the characteristics of an individual installation to work as a distortion filter.

Future investigations will include impedance and current analysis to deduce if passive filter components or active current injections by control or a mixture of both cause the observed behavior.

CRediT authorship contribution statement

Ellen Förstner: Writing – review & editing, Writing – original draft, Visualization, Supervision, Software, Project administration, Methodology, Investigation, Formal analysis, Conceptualization. **Mohamad Dughmosh:** Writing – original draft, Visualization, Validation, Software, Methodology, Investigation, Formal analysis. **Ralf Mikut:** Writing – review & editing, Visualization, Methodology, Formal analysis. **Karl-Heinz Haefele:** Writing – review & editing, Writing – original draft, Visualization, Investigation, Data curation. **Denis Jakel:** Writing – original draft, Validation. **Kaibin Bao:** Writing – original draft, Resources, Investigation. **Heiko Maaß:** Writing – review & editing, Supervision, Software, Resources, Data curation. **Richard Jumar:** Software, Resources, Data curation. **Andreas Fotler:** Validation, Software, Investigation, Formal analysis. **Uwe Kühnapfel:** Writing – review & editing, Funding acquisition. **Veit Hagenmeyer:** Writing – review & editing, Funding acquisition, Conceptualization.

Declaration of competing interest

The authors declare that they have no known competing financial interests or personal relationships that could have appeared to influence the work reported in this paper.

Acknowledgments

The authors would like to thank their colleagues from Energy Lab 2.0 and the Institute for Automation and Applied Informatics (IAI) for their continuous support in setting up and executing the field measurement. We especially thank Alexander Höllhuber, Franz-Josef Kaiser, and Andreas Hofmann.

Funding: This work is carried out within the Energy System Design (ESD) program of the Helmholtz Association of German Research Centers at Karlsruhe Institute of Technology (KIT).

Data availability

Measured data as well as analysis scripts used for this paper are available at https://doi.org/10.5281/zenodo.16306034 [20].

References

[1] Li C. Unstable operation of photovoltaic inverter from field experiences. IEEE Trans Power Deliv 2018;33(2):1013–5. http://dx.doi.org/10.1109/TPWRD.2017.2656020.

[2] Wachter J, Gröll L, Hagenmeyer V. Survey of real-world grid incidents - opportunities, arising challenges and lessons learned for the future converter dominated power system. IEEE Open J Power Electron 2024;5:50–69. http://dx.doi.org/10.1109/OJPEL.2023.3343167.

[3] De Rua P, Roose T, Sakinci ÖC, de Morais Dias Campos N, Beerten J. Identification of mechanisms behind converter-related issues in power systems based on an overview of real-life events. Renew Sustain Energy Rev 2023;183:113431. http://dx.doi.org/10.1016/j.rser.2023.113431.

[4] Kalair A, Abas N, Kalair AR, Saleem Z, Khan N. Review of harmonic analysis, modeling and mitigation techniques. Renew Sustain Energy Rev 2017;78:1152–87. http://dx.doi.org/10.1016/j.rser.2017.04.121.

[5] Messo T, Jokipii J, Aapro A, Suntio T. Time and frequency-domain evidence on power quality issues caused by grid-connected three-phase photovoltaic inverters. In: 16th European conference on power electronics and applications. 2014, p. 1–9. http://dx.doi.org/10.1109/EPE.2014.6910808.

[6] Acero JFC, Viveros HP, Castañón NJB, Yucra RC. Improvement of power quality for operation of the grid-connected photovoltaic energy system considering the irradiance uncertainty. In: IEEE XXVII international conference on electronics, electrical engineering and computing. 2020, p. 1–4. http://dx.doi.org/10.1109/INTERCON50315.2020.9220222.

[7] Al-Majidi SD, Al-Nussairi MK, Rashed JR, Abbod MF. Assessment of rooftop photovoltaic installations on the total harmonic distortion of low voltage distribution networks. In: 56th international universities power engineering conference. 2021, p. 1–5. http://dx.doi.org/10.1109/UPEC50034.2021.9548229.

[8] Alawasa KM, Al-Odienat AI. Power quality investigation of single phase grid-connected inverter of photovoltaic system. J Eng Technol Sci 2019;51(5):597–614. http://dx.doi.org/10.5614/j.eng.technol.sci.2019.51.5.1.

[9] Adebiyi AA, Davidson IE. Analysis of solar irradiation impact on grid-tied photovoltaic systems' power quality characteristics. In: 31st southern african universities power engineering conference. 2023, p. 1–5. http://dx.doi.org/10.1109/SAUPEC57889.2023.10057766.

[10] Seme S, Lukač N, Štumberger B, Hadžiselimović M. Power quality experimental analysis of grid-connected photovoltaic systems in urban distribution networks. Energy 2017;139:1261–6. http://dx.doi.org/10.1016/j.energy.2017.05.088.

[11] Ahmed N, Sedky A, Fatehy A, Foda M. Impact of grid-connected photovoltaic system on power-quality indices and its output variations with temperature. CIRED - Open Access Proc J 2017;2017:710–4. http://dx.doi.org/10.1049/oap-cired.2017.0132.

[12] Barbu V, Chicco G, Corona F, Golovanov N, Spertino F. Impact of a photovoltaic plant connected to the MV network on harmonic distortion: An experimental assessment. UPB Sci Bull Ser C: Electr Eng 2013;75:179–93.

[13] Urbanetz J, Braun P, Rüther R. Power quality analysis of grid-connected solar photovoltaic generators in Brazil. Energy Convers Manage 2012;64:8–14. http://dx.doi.org/10.1016/j.enconman.2012.05.008.

[14] Maass H, Çakmak HK, Bach F, Kühnapfel UG. Preparing the electrical data recorder for comparative power network measurements. In: IEEE international energy conference. IEEE; 2014, p. 759–65. http://dx.doi.org/10.1109/ENERGYCON.2014.6850511.

[15] Maaß H, Cakmak HK, Bach F, Mikut R, Harrabi A, Süß W, Jakob W, Stucky K-U, Kühnapfel UG, Hagenmeyer V. Data processing of high-rate low-voltage distribution grid recordings for smart grid monitoring and analysis. EURASIP J Adv Signal Process 2015;2015(1):14. http://dx.doi.org/10.1186/s13634-015-0203-4.

[16] Müller N, Bao K, Matthes J, Heussen K. CyPhERS: A cyber-physical event reasoning system providing real-time situational awareness for attack and fault response. Comput Ind 2023;151:103982. http://dx.doi.org/10.1016/j.compind.2023.103982.

[17] Müller N, Bao K, Heussen K. Cyber-physical event reasoning for distributed energy resources. Sustain Energy, Grids Netw 2024;39:101400. http://dx.doi.org/10.1016/j.segan.2024.101400.

[18] SMASolar Technology AG. SMA safety and password concept for password-protected PV plants with Bluetooth wireless technology. 2025, URL https://files.sma.de/downloads/Sicherheit-TEN103010.pdf, [last Accessed 08 August 2025].

[19] The MathWorks Inc. MATLAB version: 23.2.0.2365128 (R2023b). 2023, URL https://www.mathworks.com, [last Accessed 08 August 2025].

[20] Förstner E, Heiko M, Dughmosh M, Mikut R, Haefele K-H, Jakel D, Bao K, Jumar R, Fotler A, Kühnapfel U, Hagenmeyer V. Dataset on the Impact of a Photovoltaic Installation on Distribution Grid Voltage Waveform Distortions. 2026, http://dx.doi.org/10.5281/zenodo.16306034, [Data set], Zenodo.

[21] IEC 61000-4-7:2002 + A1:2008. Electromagnetic compatibility (EMC) - Part 4-7: Testing and measurement techniques - General guide on harmonics and interharmonics measurements and instrumentation, for power supply systems and equipment connected thereto. Standard, International Electrotechnical Commission; 2008.

[22] Prabhu KMM. Window functions and their applications in signal processing. Taylor & Francis; 2014, http://dx.doi.org/10.1201/9781315216386.

[23] Langella R, Testa A, Meyer J, Möller F, Stiegler R, Djokic SZ. Experimental-Based Evaluation of PV Inverter Harmonic and Interharmonic Distortion Due to Different Operating Conditions. IEEE T Instrum Meas 2016;65(10):2221–33. http://dx.doi.org/10.1109/TIM.2016.2554378.

[24] Alhafadhi L, Teh J. Advances in reduction of total harmonic distortion in solar photovoltaic systems: A literature review. Int J Energy Res 2020;44:2455–70. http://dx.doi.org/10.1002/er.5075.

[25] Maity S, Rather ZH, Doolla S. A comprehensive review of grid support services from solar photovoltaic power plants. Renew Sustain Energy Rev 2025;210:115133. http://dx.doi.org/10.1016/j.rser.2024.115133.